Published in final edited form as:
J Toxicol Environ Health A. 2012 January 15; 75(2): 112–128. doi:10.1080/15287394.2011.615110.

Cell Permeability, Migration, and Reactive Oxygen Species Induced by Multi-Walled Carbon Nanotubes in Human Microvascular Endothelial Cells

M Pacurari[1], **Y Qian**[2,*], **W Fu**[3], **D Schwegler-Berry**[2], **M Ding**[2], **V Castranova**[1,2], and **NL Guo**[1,4,*]

[1]Mary Babb Randolph Cancer Center, West Virginia University, Morgantown, WV 26506

[2]Pathology and Physiology Research Branch, Health Effects Laboratory Division, National Institute for Occupational Safety and Health, Morgantown, WV 26505

[3]Department of Biochemistry, West Virginia University, Morgantown, WV 26506

[4]Department of Community Medicine, School of Medicine, West Virginia University, Morgantown, WV 26506

Abstract

Multi-walled carbon nanotubes (MWCNT) have elicited great interest in biomedical applications due to their extraordinary physical, chemical, and optical properties. Intravenous administration of MWCNT-based medical imaging agents and drugs in animal models was utilized. However, the potential harmful health effects of MWCNT administration in humans have not yet been elucidated. Furthermore, to date, there are no apparent reports regarding the precise mechanisms of translocation of MWCNT into target tissues and organs from blood circulation. This study demonstrates that exposure to MWCNT leads to an increase in cell permeability in human microvascular endothelial cells (HMVEC). The results obtained from this study also showed that the MWCNT-induced rise in endothelial permeability is mediated by reactive oxygen species (ROS) production and actin filament remodeling. In addition, it was found that MWCNT promoted cell migration in HMVEC. Mechanistically, MWCNT exposure elevated the levels of monocyte chemoattractant protein-1 (MCP-1) and intercellular adhesion molecule 1 (ICAM-1) in HMVEC. Taken together, these results provide new insights into the bioreactivity of MWCNT, which may have implications in the biomedical application of MWCNT in vascular targeting, imaging, and drug delivery. The results generated from this study also elucidate the potential adverse effects of MWCNT exposure on humans at the cellular level.

Keywords

nanoparticles; molecular biology; oxidative stress; endothelium; cell morphology

[*]Corresponding authors: Nancy L. Guo, Mary Babb Randolph Cancer Center and Department of Community Medicine, West Virginia University, Morgantown, WV 26506-9300, Tel: (304) 293-6455; Fax: (304) 293-4667; lguo@hsc.wvu.edu and Yong Qian, Pathology and Physiology Research Branch, Health Effects Laboratory Division, National Institute for Occupational Safety and Health, 1095 Willowdale Road, Morgantown, WV 26505-2888, Tel: (304) 285-6286; Fax: (304) 285-5938; yaq2@cdc.gov.

Introduction

Since their discovery in 1991 by Iijma (1991), carbon nanotubes (CNT) have become one of the predominant nanoparticles with a broad application in many industries, including, but not limited to, supercapacitors, batteries, automotive industry, aerospace industry, electronics, pharmaceutics, bio-engineering, medical devices, and biomedicine (Aschberger et al., 2010). CNT are engineered either as single-walled carbon nanotubes (SWCNT) or multi-walled carbon nanotubes (MWCNT). SWCNT exist as a single sheet of graphene rolled-up in the form of a cylinder with a nanoscale diameter and lengths ranging up to several μm, whereas MWCNT are multiple SWCNT within SWCNT with diameters up to 100 nm and lengths up to several μm (Pacurari et al., 2010). Structurally, MWCNT resemble seamless cylinders of rolled-up sheets of graphene concentrically stacked one inside the other. MWCNT have been applied in many industrial areas due to their small size, light weight, large surface area, stability, rigidity, and electrical and optical properties (Kis and Zettl, 2008). Particularly, MWCNT have shown a great potential in biomedical applications, such as imaging and diagnosis, targeted therapeutic modalities, thermal cancer treatment, and tumor vasculature targeting (Burke et al., 2009; Kostarelos et al., 2009; Ruggiero et al., 2010a).

An animal study showed that MWCNT-mediated delivery of drugs leads to successful and statistically significant suppression of tumor volume, followed by a concomitant prolongation of survival of human lung tumor-bearing animals (Podesta et al., 2009). This study also indicated the potential advantages of MWCNT-based drug delivery for the intracellular delivery of therapeutic agents in vivo in comparison with other drug delivery systems. Studies investigating pharmacokinetic properties of chemically modified MWCNT indicated that the systemic delivery of MWCNT has promising potential for the development of diagnostic and therapeutic tools for both cardiovascular diseases and cancer (Lacerda et al., 2008; Podesta et al., 2009; Ruggiero et al., 2010b; Singh et al., 2006). It was found that functionalized MWCNT translocate from blood circulation into organs after intravenous (IV) administration (Deng et al., 2007; Guo et al., 2007), and are biopersistent in vivo for a long period of time (Deng et al., 2007). However, the mechanisms by which MWCNT cross the endothelium from circulating blood into underlying organs have not been fully elucidated.

Concerns over potential MWCNT-induced harmful health effects in humans have been raised primarily due to their fibrous-like structure (Johnston et al., 2010; Poland et al., 2008; Takagi et al., 2008). Kane (1996) found that exposure to long fibers is associated with chronic lung lesions in humans. Studies in animal models showed that exposure to long fibers induced fibrogenic inflammatory and carcinogenic responses (Davis et al., 1986; Davis and Jones, 1988).

A potential for adverse health effects has also been raised due to the biopersistence of MWCNT. MWCNT tend to persist in vivo due to their resistance to high temperature or acid treatment (Johnston et al., 2010; Pacurari et al., 2010; Poland et al., 2008). Therefore, it was proposed that MWCNT may potentially induce pathogenic and/or carcinogenic effects (Donaldson et al., 2006; Kane and Hurt, 2008). Indeed, in vivo studies reported that MWCNT induced inflammation, granuloma formation, and persistent interstitial fibrosis (Porter et al., 2010; Takagi et al., 2008). Following intraperitonael (IP) administration, Aiso et al (2010; 2011) demonstrated that MWCNT were detected in the lung 60 days post-exposure. In vitro studies showed that exposure of lung and skin cells to MWCNT induced cytotoxic effects, oxidative stress, and genotoxic effects (Asakura et al., 2010; Patlolla et al., 2010; Wang et al., 2010).

Branchaud et al. (1989) demonstrated that exposure to fibrous particles induced adverse effects on the vascular system. A study found that injection of asbestos fibers into mice induced angiogenesis around clusters of asbestos, which may facilitate the later emergence of mesotheliomas (Branchaud et al., 1989). Other in vivo and in vitro studies demonstrated that fiber exposure induced an increase in vascular permeability, leukocyte extravasation, small vessel remodeling, and angiogenesis (Barchowsky et al., 1997; Hamilton, 1983), which may involve reactive oxygen species (ROS)-dependent signaling pathways (Garcia et al., 1989). Barchowsky et al. (1997; 1998) also found that exposure of endothelial cells to fibrous particles resulted in altered cell morphology, an elevation in ICAM-1, urokinase-type plasminogen activator (uPA) and its receptor uPAR expression, and activation of focal adhesion kinases (FAK). Given the fibrous-like structures and biopersistence of MWCNT, it is possible that MWCNT exposure through systemic administration, as well as inhalation, may induce endothelial injury.

The vascular endothelial cells form a semi-selective permeability barrier between circulating blood and the interstitial tissues. This barrier controls the transport of fluids, electrolytes and macromolecules across the vessel wall. Any change in endothelial cell permeability might play an important role in the development of a variety of diseases including cardiovascular diseases, inflammatory diseases, diabetic vascular complications, acute lung injury, and metastasis. Nevertheless, alterations of endothelial permeability are important features in selective drug delivery therapies (Fang et al., 2011). Although MWCNT exposure was shown to induce adverse effects in numerous cells, whether exposure of endothelial cells to MWCNT may induce endothelial injury is unknown. This study sought to investigate the effects of MWCNT exposure on human microvascular endothelial cells (HMVEC). Studies were undertaken to examine whether MWCNT exposure induced an increase in permeability and migration in HMVEC and to determine the underlying molecular mechanisms involved. Specifically, assays were conducted to determine the involvement of MWCNT-induced ROS production in endothelial permeability and migration changes.

Materials and Methods

MWCNT

The MWCNT used in the present study were a gift from Mitsui-&-Company (MWCNT-7, lot # 05072001K28). The characterization of MWCNT was previously published (Porter et al., 2010). Briefly, the bulk MWCNT exhibit a distinctive crystalline structure with the number of walls ranging from 20 to 50. Overall, MWCNT trace metal contamination was 0.78%, including sodium (0.41%) and iron (Fe) (0.32%) with no other metals present above 0.02%. Transmission electron microscopy (TEM) micrographs of MWCNT dispersed in dispersion medium (DM; Ca^{2+} and Mg^{2+}-free phosphate buffered saline, pH 7.4, supplemented with 5.5 mM d-glucose, 0.6 mg/ml mouse serum albumin, and 0.01 mg/ml 1,2-dipalmitoyl-sn-glycero-3-phosphocholine) demonstrated that DM promotes significant dispersion of MWCNT (Porter et al., 2008). The quantitative analysis of TEM micrographs revealed that the median length of this MWCNT sample was 3.86 μm (GSD 1.94) and the count mean width was 49 ±13.4 (S.D.) nm. The zeta potential (ZP) of the MWCNT in the DM was determined to be -11mV (Porter et al., 2010). The ZP is an indicator of particle movement in a solution under an electric field (Banerjee et al., 1996).

MWCNT preparation

For cell culture studies, MWCNT were prepared in DM (Porter et al., 2008). Briefly, DM consists of Ca^{2+}/Mg^{2+}-free phosphate-buffered saline (PBS), pH 7.4, supplemented with 5.5 mM D-glucose, 0.6 mg/ml mouse serum albumin, and 0.01 mg/ml 1,2-dipalmitoyl-sn-glycero-3-phosphocholine (DPPC). DPPC was prepared fresh as a 10 mg/ml stock solution

in absolute ethanol. MWCNT were prepared in DM followed by indirect sonication at 4°C for 5 min (Hielscher ultrasonic processor, UIS259L) at amplitutide 100% and cycle 1. After the indirect sonication, the suspension was direct sonicated at 4°C for 5 min at 5W output and 10% duty cycle (Branson Sonifier 450). The stock solution (1 mg/ml) of MWCNT was kept at 4°C and used within 2-3 weeks. Prior to cell culture experiments, the MWCNT stock solution was directly sonicated for 1 min at the setting indicated above.

Cell culture

HMVEC were a kind gift from Dr. Rong Shao (Biomedical Research Institute, Baystate Medical Center/University of Massachusetts, Amherst, Springfield, MA). HMVEC were cultured according to the protocol described previously (Shao and Guo, 2004). Briefly, HMVEC were grown in endothelial basal medium-2 (EBM-2) (Lonza, Boston, MA) supplemented with 10% (v/v) fetal bovine serum (FBS) (Atlanta Biologicals, Lawrenceville, GA), 100 U/ml penicillin, 10 μg/ml streptomycin, 0.01 μg/ml epidermal growth factor, and 1 μg/ml hydrocortisone. The cells were maintained in an incubator at 37°C with 5% CO_2 in air.

Transendothelial electrical resistance (TER)

The TER was measured using an electrical cell-substrate impedance sensing system (ECIS) (Applied Biophysics, Troy, NY) according to the published protocol (Apopa et al., 2009). TER is a measure of endothelial barrier integrity. Briefly, HMVEC were grown to confluent monolayers on ECIS culture ware and serum starved overnight. The electrical resistance was measured on cells located on the small gold electrodes in each of the wells. The culture medium was the electrolyte. The small gold electrode covered by confluent HMVEC and a larger gold counter electrode were connected to a phase-sensitive lock-in amplifier. A constant current of 1 μA was supplied by a 1-V, 4000-Hz alternating current through a 1-MÙ resistor. Changes in voltage between the small electrode and the large counter electrode were continuously monitored by the lock-in amplifier, stored, and then used to calculate resistance.

Immunofluorescence assay

Immunofluorescence assays were applied to measure MWCNT-induced changes in endothelial permeability and actin filament remodeling, which were performed according to methods previously published (Qian et al., 2005; 2010). Briefly, HMVEC were grown on cover slips to 100% confluence, followed by MWCNT treatment. After treatments, cells were washed with phosphate-buffered saline (PBS), fixed with 4% paraformaldehyde, permeabilized in 0.1% Triton X-100/PBS for 4 min, blocked in 5% BSA/PBS for 1 hr, and incubated with specific primary antibodies overnight at 4°C, followed by incubation with immunofluorescence-conjugated secondary antibodies at room temperature for 1 hr. The labeled cover slips were then mounted to the slides with an antifade reagent (Invitrogen, Eugene, OR). A Zeiss LSM 510 microscope was used to obtain images. Scale bars were generated and inserted using LSM software.

Measurement of ROS production

The measurements of ROS production by confocal microscopy were performed according to the methods previously described (Qian et al., 2005). Briefly, cells were grown on cover slips until 100% confluent, serum-starved overnight, and then exposed to 2.5 μg/ml MWCNT for different periods of time. Some experiments were performed with a ROS scavenger, catalase (Sigma Aldrich, St. Louis, MO). For these experiments, the cells were pretreated with catalase (1000 U/ml) during the last 30 min of treatments as indicated. During the exposure periods, dihydroethidium (DHE; a probe for $O_2^{\cdot-}$) was added at a final

concentration of 5 μM for the last 30 min of exposure. After incubation, the cells were washed twice with PBS, fixed with 4% paraformaldehyde, permeabilized with 0.1% Triton X-100/PBS, washed thrice with PBS, and mounted on slides with an antifade reagent (Invitrogen). A Zeiss LSM 510 microscope was used to obtain images. Scale bars were generated and inserted using LSM software. DHE fluorescence intensity was quantified on the acquired images using an automated image analysis system (Optimas 6.51, Media Cybernetics Inc., Silver Spring, Md). A minimum of 20 cells were scored for each sample from three independent experiments. Data are presented as mean ± SEM.

Transmission electron microscopy (TEM)

The uptake of MWCNT by HMVEC was analyzed by TEM according to the previously described procedure (Apopa et al., 2009). Briefly, HMVEC were grown to confluence and exposed to MWCNT (2.5 μg/ml) for various periods of time, washed with ice cold $Ca^{2+/}Mg^{2+}$-free PBS, scraped from the wells, and harvested by centrifugation at 700 rpm (109 g) for 5 min. The cells were fixed in Karnovsky's fixative (2.5% glutaraldehyde + 3% paraformaldehyde in 0.1 M sodium cacodylate, pH 7.4), washed thrice in 0.1 M sodium cacodylate and post-fixed in 1% osmium tetraoxide, followed by washing with 0.1 M sodium cacodylate and distilled water. The cells were dehydrated by sequential washings in 25, 50, and 100% ethanol then embedded in LX-112 (Ladd, Williston, VT). The ultrathin sections were stained with uranyl acetate and lead citrate and examined with TEM (JEOL 1220, Tokyo, Japan).

Cell migration assay

The cell migration assay was performed according to methods previously described (Qian et al., 2005). In brief, HMVEC cells were grown on cover slips to a confluent monolayer and then scratched to form a 100-μm “wound” using sterile pipette tips. The cells were treated with 2.5 μg/ml MWCNT in serum-free media for 24 hr, fixed, and stained with crystal violet for 10 min at room temperature followed by washing with PBS. Samples were imaged using an Olympus IX70 microscope (Olympus Optical Co., Ltd, Japan) equipped with a Retiga 2000R FAST camera (Qimaging, Canada). Images were acquired using SimplePCI software (Compix Inc., Sewickley, PA). The number of cells that migrated toward the wound was counted on the acquired images from three independent experiments. Data are presented as mean ± SEM of three independent experiments.

Enzyme-Linked Immunosorbent Assay

MCP-1 and ICAM-1 levels were measured on conditioned cell culture supernatants using quantitative ELISA kits (Invitrogen™, Camarillo, CA) according to the manufacturer's protocols. Briefly, HMVEC cells (1×10^5) were grown in 12-well plates to a confluent monolayer and then exposed to 2.5 μg/ml MWCNT for 24 hr in serum free media. After 24 hr, the cell conditioned medium was collected on ice, centrifuged at 14,000 × g for 15 min, transferred to new microcentrifuge tubes, and stored at -80° C until analysis. ICAM-1 and MCP-1 levels were analyzed with a SPECTRAmax M2 microplate reader running SoftMax Pro software (Molecular Devices, Sunnyvale, CA) according to the manufacturer's protocols (Invitrogen).

Statistical analysis

Data are presented as mean ± SEM from three experiments. Statistical analysis was performed using one-way analysis of variance (ANOVA) and Student's paired *t*-test with a significance level of $p \leq 05$ versus non-treated control samples.

Results

MWCNT uptake by HMVEC

Previously, it was found that MWCNT are taken up by human epidermal keratinocytes (Monteiro-Riviere et al., 2005). The current study sought to investigate whether HMVEC might possess an ability to take up MWCNT. HMVEC were grown to a confluent monolayer, and then were exposed to 2.5 μg/ml of MWCNT for different periods of time ranging from 30 min to 24 hr. After the exposure, cells were processed for TEM analysis. As shown in Figure 1B, MWCNT particles were found in close contact with the surface of HMVEC at 30 min of exposure. At 1 hr exposure, the particles were found in the cytoplasm of HMVEC, indicating that the cells were able to take up MWCNT (Figures 1B and 1C). By 4 to 8 hr, the uptake of MWCNT by HMVEC increased (Figures 1D and 1E). The uptake of MWCNT lasted through at least 24 hr exposure in HMVEC (Figure 1F). Approximately, 50% of the cells examined by TEM engulfed MWCNT within 24 hr after exposure (data not shown). These results demonstrate that HMVEC displays an ability to take up MWCNT into the cells.

MWCNT increase HMVEC cell permeability

Confluent HMVEC were exposed to 2.5 μg/ml of MWCNT for different periods of time, followed by confocal microscopy imaging analysis. The results show that the untreated cells were closely attached with no substantial amounts of gaps in the HMVEC monolayer (Figure 2A). Conversely, the MWCNT-exposed HMVEC monolayers were pulled apart to form gaps as early as 1 hr after exposure (Figure 2A). The increase in gap formation persisted up to 24 hr (Figure 2A). Concentration- and time-dependent experiments were also performed to identify the concentration range of MWCNT in inducing the HMVEC monolayer change. The results demonstrated that MWCNT concentrations greater than 2.5 μg/ml induced more predominant gaps (data not shown). Since our cell viability assays showed that concentrations in excess of 2.5 μg/ml of MWCNT significantly reduced cell viability (data not shown), the concentration of 2.5 μg/ml was selected for this study.

Transendothelial electrical resistance (TER) measurements were then applied to verify the MWCNT-induced effect on HMVEC permeability. TER is a highly sensitive measurement of endothelial cell permeability, and the change in TER reading inversely correlates with an increase in cell permeability. The results of this assay demonstrated that exposure of HMVEC to MWCNT decreased the TER of HMVEC monolayer over 50 hr of exposure time (Figure 2B), indicating that the monolayer was compromised and endothelial cell permeability rose. Taken together, the results demonstrated that MWCNT exposure displayed an ability to increase endothelial cell permeability in HMVEC.

MWCNT induce the production of ROS in HMVEC

The production of ROS was investigated using confocal microscopy by measuring changes in the fluorescence of DHE. HMVEC were exposed to 2.5 μg/ml MWCNT for different periods of time, followed by incubation with DHE for the last 30 min of exposure. The results show that a significant increase in ROS production started at 1 hr of exposure, peaked at 8 hr, and declined somewhat at 24 hr while the untreated control cells showed a low basal level of ROS production (Figures 3A and 3B). To exclude the possibility that the trace metal contamination of Fe in MWCNT may induce ROS intrinsically, ROS production was measured in cell free systems (cell culture media without HMVEC). The results demonstrated that MWCNT were not able to produce ROS intrinsically (Figure 3C). To verify the specificity of ROS production, catalase (1000 U/ml), a ROS scavenger, was applied to pretreat the cells for 1 hr, followed by exposure to MWCNT for 8 hr. The results show that pretreatment with catalase significantly prevented MWCNT-induced ROS

generation in HMVEC (Figures 3D and 3E). Taken together, the results obtained demonstrated that MWCNT exposure induced production of ROS in HMVEC.

MWCNT induce actin filament remodeling in HMVEC

In the present study, confocal microscopy imaging analysis was applied to investigate MWCNT exposure-induced effects on actin filament remodeling in HMVEC. The HMVEC monolayer was exposed to 2.5 μg/ml MWCNT for different periods of time and the integrity of actin filament network was determined using FITC-phalloidin staining, followed by confocal microscopy imaging analysis. As shown in Figure 4, in untreated HMVEC, actin filaments were evenly distributed throughout cells to form a well-organized network structure and no significant amounts of cell peripheral motile structures were found. Within 1 hr of MWCNT exposure, actin filaments were remodeled to form peripheral motile structures, lamellipodia and filopodia, and central actin filament bundles. Moreover, the cells were pulled apart to form small gaps in the HMVEC monolayer. MWCNT-induced effects on actin filaments lasted more than 8 hr and declined 24 hr after the exposure. Interestingly, actin filament staining showed more intercellular gaps were found at 24 hr post exposure (Figure 4). The results demonstrated that MWCNT exposure induced actin filament remodeling in HMVEC.

MWCNT induce actin filament remodeling and permeability through the production of ROS in HMVEC

The cells were pretreated with catalase, a specific ROS scavenger, followed by MWCNT treatment and confocal microscopy analysis. The results show that the removal of ROS with catalase inhibited MWCNT-induced intercellular gap formation in the HMVEC monolayer (Figure 5A). These results indicate that the production ROS may mediate MWCNT-induced permeability in HMVEC. Confocal microscopy imaging analysis was also applied to determine the regulatory role of ROS production in MWCNT-induced actin filament remodeling. The HMVEC monolayer was pretreated with catalase for 1 hr, followed by exposure to 2.5 μg/ml MWCNT for 1 hr. The results show that catalase pretreatment inhibited MWCNT-induced actin filament remodeling, indicating that the production of ROS plays a regulatory role in this process (Figure 5B). Taken together, these results demonstrated that the production of ROS played an essential role in modulating MWCNT-induced actin filament remodeling and enhanced permeability in HMVEC.

MWCNT induce an increase in migration in HMVEC

The HMVEC monolayer was scratched to form a 100-μm wound with sterile pipette tips, followed by exposure to 2.5 μg/ml MWCNT for 24 hr. The results show that MWCNT-exposed cells at the edge of the wound migrated and spread to heal the wound faster than the untreated cells (Figures 6A and 6B). A significant number of cells were found in the wound area in MWCNT exposed endothelial cells compared to untreated control cells (Figures 6A, 6B, and 6D). The results indicate that MWCNT modulate endothelial cell behavior and induce an increase in HMVEC migration. Moreover, the removal of ROS by catalase pretreatment blocked MWCNT-induced migration, indicating that the production of ROS plays a regulatory role in MWCNT-induced migration (Figures 6C and 6D).

MWCNT induce the production of MCP-1 and ICAM-1 in HMVEC

As shown in Figure 7, HMVEC exposure to 2.5 μg/ml MWCNT induced the production of MCP-1 (Figure 7A) at 24 hr after exposure and ICAM-1 (Figure 7B) at 8 hr after exposure.

Discussion

Two pathways are involved in the control of substance transfer through the endothelial semi-permeable barrier: transcellular and paracellular pathways (Mehta and Malik, 2006). The transcellular pathway controls the transport of macromolecules via endocytosis in vesicle carriers. The paracellular pathway mediates the passage of macromolecules via the opening and closing of endothelial cell-cell junctions and transendothelial permeability changes, which are a coordinated processes regulated by cellular cytoskeleton contractile forces, cell-cell junctions, and cell-adhesion junctions (Mehta and Malik, 2006). The unperturbed endothelial paracellular pathway allows the passive passage of substances with a radius of less than 3 nm through the barrier. However, upon stimulation, the perturbed endothelial paracellular pathway becomes leaky and forms gaps between the endothelial cells to allow the passage of larger molecules (Mehta and Malik, 2006). It was reported that CNT cross the endothelial semi-permeable barrier via the transcellular pathway (Bianco et al., 2005; Jin et al., 2008; Pantarotto et al., 2004). In the present study, the results demonstrated that MWCNT induced an increase in endothelial cell permeability. The results of transendothelial electrical resistance (TER) measurements indicate that the increase in endothelial permeability may occur right after the exposure, accelerate around 10 hours after the exposure, and last at least 50 hours. Indeed, the image analysis data of both VE-cadherin and actin filament staining showed that the formation of MWCNT-induced gaps occurred as early as 1 hour after the exposure, peaked around 8 hours after the exposure and lasted at least 24 hours (Figures 2A and 4). This finding suggests that MWNCT may potentially promote vascular extravasation and be translocated into the underlying surrounding tissues and organs in vivo via changes in the paracellular pathway, specifically, permeability modulation. Indeed, animal studies found that upon exposure via IV injection, MWCNT were detected in various distant organs in both mice and rat (Deng et al., 2007; Lacerda et al., 2008).

The concentration (2.5 μg/ml) of MWCNT used in this study is comparable to the concentrations used in the studies of systemic administration of MWCNT for imaging, bio-distribution, translocation, and direct tumor injection. Lacerda et al. (2008) injected 300 μg MWCNT per rat, which translates to a concentration of 20 μg/ml (average rat blood volume 15 ml and 200 g body weight). Deng et al. (2007) injected 10 μg MWCNT per mouse, which translates to a concentration of 10 μg/ml (average mouse blood volume 1 ml and 20 g body weight). It appears that these animal imaging studies of systemic administration of functionalized and radiolabeled MWCNT utilized higher doses of MWCNT than the current in vitro endothelial-based study. Our unpublished data indicate that concentrations of MWCNT above 2.5 μg/ml induce cellular toxicity in vitro. Therefore, the concentration applied in this study may represent a ceiling for the non-cytotoxic level, which may be useful to guide future in vivo applications of MWCNT in biomedicine.

Several studies have demonstrated that many nanoparticles have an ability to induce the production of ROS (Nel et al., 2006). ROS-induced acute and chronic oxidative stress can cause vascular endothelial dysfunction, which plays an important role in the pathophysiology of various vascular diseases and disorders (Lum and Roebuck, 2001). In this study, it was found that MWCNT exposure induced the production of ROS in HMVEC. These results are consistent with our previous observations of Fe nanoparticle-induced ROS production in endothelial cells (Apopa et al., 2009). One of the unique features of nanoparticles is small particle size with a large surface area. As a consequence, more atoms are exposed on the particle surface instead of occluded within the interior of the material. Therefore, their electronic properties are altered, which may serve as reactive sites for ROS production (Nel et al., 2006). Indeed, in vivo studies demonstrated a direct relationship between the surface area of nanoparticles, ROS-generating capability, and proinflammatory

effects in the lung (Nel et al., 2006). Numerous studies showed that the production of ROS is a major mechanism for the induction of nanoparticle-related adverse biological effects (Gwinn and Vallyathan, 2006; Nel et al., 2006). Gwinn and Vallyathan (2006) indicated that nanoparticle-induced ROS production leads to the activation of cellular signaling pathways and apoptosis, which is directly related to the development of nanoparticle-induced pulmonary injury and other diseases. In this study, the results show that MWCNT-induced ROS play a regulatory role in endothelial permeability, as well as migration. The production of ROS is directly related to the increase in permeability and migration in endothelial cells (Houle and Huot, 2006; Lum and Roebuck, 2001; Qian et al., 2005). Endothelium-based hyperpermeability and migration are two key steps of vascular remodeling, which is directly involved in inflammation, fibrosis, and cancer (Hassoun et al., 2009; Strieter and Mehrad, 2009; Wallace et al., 2007). The results generated from this study may elucidate a molecular mechanism that may be related to MWCNT-induced pulmonary inflammation, and particularly, fibrosis.

Actin filaments are dynamic intracellular structures that undergo constant remodeling, which form central stress fibers for substratum anchorage and the peripheral structures of lamellipodia and filopodia for cell spreading and migration (Gotlieb, 1990). They are key components of cell junctions and adhesions, serve as contractile apparatuses, and play a critical role in modulating endothelial cell permeability (Dudek and Garcia, 2001; Shasby et al., 1982). Disruption of actin filaments is directly related to an increase in endothelial cell permeability (Mehta and Malik, 2006). This study demonstrates that MWCNT exposure induced actin filament remodeling, which may indicate a potential molecular mechanism by which MWCNT increase endothelial permeability and migration. The results of MWCNT-induced actin filament remodeling also indicate that MWCNT have the ability to induce cell migration. Cell migration is a multistep process in which the actin filament-based cytoskeleton plays a key role (Lee and Gotlieb, 2003). Indeed, the results of this study demonstrate that MWCNT have an ability to induce endothelial migration, which is consistent with the published observations of MWCNT-induced cell migration. It was found that MWCNT modulate cell adhesion and migration in MWCNT-coated composites and implanted biomedical apparatuses (Hirata et al., 2009; Misra et al., 2010; Raffa et al., 2009; Wang et al., 2007). The results of the cell migration assay obtained in this study are comparable to the effects of MWCNT on fibroblast proliferation, osteoblast proliferation, bone grafting, and nerve regeneration (Christenson et al., 2007; Ding et al., 2005; Li et al., 2009; Yadav et al., 2010). The increased expression of MCP-1 and ICAM-1 observed in this study may indicate the potential molecular mechanisms involved in MWCNT-induced endothelial migration. The role of MCP-1 in facilitating endothelial cell migration was previously shown (Weber et al., 1999). ICAM-1 plays an important role in transducing extracellular signals, transendothelial leukocyte migration and lung cancer cell migration (Aghajanian et al., 2008; Chen et al., 2011). Both MCP-1 and ICAM-1 are key factors responsible for mononuclear cell recruitment, adhesion, and transendothelial migration (Gerszten et al., 1999), and play an important role in mediating cell-cell adhesion and cell migration (Weber et al., 1999).

The observed MWCNT-induced actin filament remodeling, cell migration, and permeability altogether suggest that MWCNT have an ability to induce vascular remodeling and angiogenesis. Currently, experiments are being designed to examine whether MWCNT exposure may induce an increase in angiogenesis in HMVEC.

In summary, the results of this study demonstrate that exposure to MWCNT induced an increase in endothelial monolayer permeability and migration in HMVEC. Mechanistically, MWCNT appear to induce endothelial cell permeability and migration through ROS production and actin filament remodeling. These data provide new insights concerning the

mechanisms of MWCNT interactions with the vascular endothelium, which may have implications for future applications of MWCNT in nanomedicine for vascular imaging, vascular macromolecular delivery, and drug transport. The finding that MWCNT induce permeability and migration may also indicate the mechanisms by which MWCNT translocate from the blood stream into the underlying tissue of distant organs following systemic administration. Furthermore, these results may be useful for understanding the bioreactivity of MWCNT, which inform potential applications of MWCNT in biomedicine and elucidate the possible adverse health effects in humans.

Acknowledgments

We thank Rebecca Raese for her help in editing the manuscript. This study is supported by NIH/NLM R01LM009500 (PI: Guo) and NCRR P20RR16440 and Supplement (PD: Guo).

References

Aghajanian A, Wittchen ES, Allingham MJ, Garrett TA, Burridge K. Endothelial cell junctions and the regulation of vascular permeability and leukocyte transmigration. J Thromb Haemost. 2008; 6:1453–1460. [PubMed: 18647230]

Aiso S, Kubota H, Umeda Y, Kasai T, Takaya M, Yamazaki K, Nagano K, Sakai T, Koda S, Fukushima S. Translocation of intratracheally instilled multiwall carbon nanotubes to lung-associated lymph nodes in rats. Ind Health. 2011; 49(2):215–20. [PubMed: 21173528]

Aiso S, Yamazaki K, Umeda Y, Asakura M, Kasai T, Takaya M, Toya T, Koda S, Nagano K, Arito H, Fukushima S. Pulmonary toxicity of intratracheally instilled multiwall carbon nanotubes in male Fischer 344 rats. Ind Health. 2010; 48(6):783–95. [PubMed: 20616469]

Apopa PL, Qian Y, Shao R, Guo NL, Schwegler-Berry D, Pacurari M, Porter D, Shi X, Vallyathan V, Castranova V, Flynn DC. Iron oxide nanoparticles induce human microvascular endothelial cell permeability through reactive oxygen species production and microtubule remodeling. Part Fibre Toxicol. 2009; 6:1. [PubMed: 19134195]

Asakura M, Sasaki T, Sugiyama T, Takaya M, Koda S, Nagano K, Arito H, Fukushima S. Genotoxicity and cytotoxicity of multi-wall carbon nanotubes in cultured Chinese hamster lung cells in comparison with chrysotile A fibers. J Occup Health. 2010; 52:155–166. [PubMed: 20379079]

Aschberger K, Johnston HJ, Stone V, Aitken RJ, Hankin SM, Peters SA, Tran CL, Christensen FM. Review of carbon nanotubes toxicity and exposure--appraisal of human health risk assessment based on open literature. Crit Rev Toxicol. 2010; 40:759–790. [PubMed: 20860524]

Banerjee AK, Weiner BB, Fairhurst D, Tscharnuter WW. Light scattering for measuring electrophoretic mobility in concentrated colloidal suspensions. Abstracts of Papers of the American Chemical Society. 1996; 212:42.

Barchowsky A, Lannon BM, Elmore LC, Treadwell MD. Increased focal adhesion kinase- and urokinase-type plasminogen activator receptor-associated cell signaling in endothelial cells exposed to asbestos. Environ Health Perspect. 1997; 105 5:1131–1137. [PubMed: 9400712]

Barchowsky A, Roussel RR, Krieser RJ, Mossman BT, Treadwell MD. Expression and activity of urokinase and its receptor in endothelial and pulmonary epithelial cells exposed to asbestos. Toxicol Appl Pharmacol. 1998; 152:388–396. [PubMed: 9853007]

Bianco A, Kostarelos K, Partidos CD, Prato M. Biomedical applications of functionalised carbon nanotubes. Chem Commun. 2005; (1):571–577.

Branchaud RM, MacDonald JL, Kane AB. Induction of angiogenesis by intraperitoneal injection of asbestos fibers. Faseb Journal. 1989; 3:1747–1752. [PubMed: 2467835]

Burke A, Ding X, Singh R, Kraft RA, Levi-Polyachenko N, Rylander MN, Szot C, Buchanan C, Whitney J, Fisher J, Hatcher HC, D'Agostino R Jr, Kock ND, Ajayan PM, Carroll DL, Akman S, Torti FM, Torti SV. Long-term survival following a single treatment of kidney tumors with multiwalled carbon nanotubes and near-infrared radiation. Proc Natl Acad Sci U S A. 2009; 106:12897–12902. [PubMed: 19620717]

Chen LM, Kuo CH, Lai TY, Lin YM, Su CC, Hsu HH, Tsai FJ, Tsai CH, Huang CY, Tang CH. RANKL increases migration of human lung cancer cells through intercellular adhesion molecule-1 up-regulation. J Cell Biochem. 2011; 112(3):933–41. [PubMed: 21328467]

Christenson EM, Anseth KS, van den Beucken JJ, Chan CK, Ercan B, Jansen JA, Laurencin CT, Li WJ, Murugan R, Nair LS, Ramakrishna S, Tuan RS, Webster TJ, Mikos AG. Nanobiomaterial applications in orthopedics. J Orthop Res. 2007; 25:11–22. [PubMed: 17048259]

Davis JM, Addison J, Bolton RE, Donaldson K, Jones AD, Smith T. The pathogenicity of long versus short fibre samples of amosite asbestos administered to rats by inhalation and intraperitoneal injection. Br J Exp Pathol. 1986; 67:415–430. [PubMed: 2872911]

Davis JM, Jones AD. Comparisons of the pathogenicity of long and short fibres of chrysotile asbestos in rats. Br J Exp Pathol. 1988; 69:717–737. [PubMed: 2848570]

Deng X, Jia G, Wang H, Sun H, Wang X, Yang S, Wang T, Liu Y. Translocation and fate of multi-walled carbon nanotubes in vivo. Carbon. 2007; 45:1419–1424.

Ding L, Stilwell J, Zhang T, Elboudwarej O, Jiang H, Selegue JP, Cooke PA, Gray JW, Chen FF. Molecular characterization of the cytotoxic mechanism of multiwall carbon nanotubes and nano-onions on human skin fibroblast. Nano Lett. 2005; 5:2448–2464. [PubMed: 16351195]

Donaldson K, Aitken R, Tran L, Stone V, Duffin R, Forrest G, Alexander A. Carbon nanotubes: a review of their properties in relation to pulmonary toxicology and workplace safety. Toxicol Sci. 2006; 92:5–22. [PubMed: 16484287]

Dudek SM, Garcia JG. Cytoskeletal regulation of pulmonary vascular permeability. J Appl Physiol. 2001; 91:1487–1500. [PubMed: 11568129]

Fang J, Nakamura H, Maeda H. The EPR effect: Unique features of tumor blood vessels for drug delivery, factors involved, and limitations and augmentation of the effect. Adv Drug Deliv Rev. 2011; 63(3):136–51. [PubMed: 20441782]

Garcia JG, Dodson RF, Callahan KS. Effect of environmental particulates on cultured human and bovine endothelium. Cellular injury via an oxidant-dependent pathway. Lab Invest. 1989; 61:53–61. [PubMed: 2747217]

Gerszten RE, Garcia-Zepeda EA, Lim YC, Yoshida M, Ding HA, Gimbrone MA Jr, Luster AD, Luscinskas FW, Rosenzweig A. MCP-1 and IL-8 trigger firm adhesion of monocytes to vascular endothelium under flow conditions. Nature. 1999; 398:718–723. [PubMed: 10227295]

Gotlieb AI. The endothelial cytoskeleton: organization in normal and regenerating endothelium. Toxicol Pathol. 1990; 18:603–617. [PubMed: 2091238]

Guo J, Zhang X, Li Q, Li W. Biodistribution of functionalized multiwall carbon nanotubes in mice. Nuclear Medicine and Biology. 2007; 34:579–583. [PubMed: 17591558]

Gwinn MR, Vallyathan V. Nanoparticles: health effects--pros and cons. Environ Health Perspect. 2006; 114:1818–1825. [PubMed: 17185269]

Hamilton JA. Asbestos fibers, plasma and inflammation. Environ Health Perspect. 1983; 51:281–285. [PubMed: 6641659]

Hassoun PM, Mouthon L, Barbera JA, Eddahibi S, Flores SC, Grimminger F, Jones PL, Maitland ML, Michelakis ED, Morrell NW, Newman JH, Rabinovitch M, Schermuly R, Stenmark KR, Voelkel NF, Yuan JX, Humbert M. Inflammation, growth factors, and pulmonary vascular remodeling. J Am Coll Cardiol. 2009; 54:S10–19. [PubMed: 19555853]

Hirata E, Uo M, Takita H, Akasaka T, Watari F, Yokoyama A. Development of a 3D collagen scaffold coated with multiwalled carbon nanotubes. J Biomed Mater Res B Appl Biomater. 2009; 90:629–634. [PubMed: 19213050]

Houle F, Huot J. Dysregulation of the endothelial cellular response to oxidative stress in cancer. Mol Carcinog. 2006; 45:362–367. [PubMed: 16637066]

Iijima S. Helical Microtubules of Graphitic Carbon. Nature. 1991; 354:56–58.

Jin H, Heller DA, Strano MS. Single-particle tracking of endocytosis and exocytosis of single-walled carbon nanotubes in NIH-3T3 cells. Nano Letters. 2008; 8:1577–1585. [PubMed: 18491944]

Johnston HJ, Hutchison GR, Christensen FM, Peters S, Hankin S, Aschberger K, Stone V. A critical review of the biological mechanisms underlying the in vivo and in vitro toxicity of carbon nanotubes: The contribution of physico-chemical characteristics. Nanotoxicology. 2010; 4:207–246. [PubMed: 20795897]

Kane AB. Mechanisms of mineral fibre carcinogenesis. IARC Sci Publ. 1996:11–34. [PubMed: 9101315]

Kane AB, Hurt RH. Nanotoxicology: The asbestos analogy revisited. Nature Nanotechnology. 2008; 3:378–379.

Kis A, Zettl A. Nanomechanics of carbon nanotubes. Philos Transact A Math Phys Eng Sci. 2008; 366:1591–1611. [PubMed: 18192169]

Kostarelos K, Bianco A, Prato M. Promises, facts and challenges for carbon nanotubes in imaging and therapeutics. Nat Nanotechnol. 2009; 4:627–633. [PubMed: 19809452]

Lacerda L, Soundararajan A, Singh R, Pastorin G, Al-Jamal KT, Turton J, Frederik P, Herrero MA, Bao SLA, Emfietzoglou D, Mather S, Phillips WT, Prato M, Bianco A, Goins B, Kostarelos K. Dynamic Imaging of functionalized multi-walled carbon nanotube systemic circulation and urinary excretion. Advanced Materials. 2008; 20:225–230.

Lee JSY, Gotlieb AI. Understanding the role of the cytoskeleton in the complex regulation of the endothelial repair. Histology and Histopathology. 2003; 18:879–887. [PubMed: 12792900]

Li X, Gao H, Uo M, Sato Y, Akasaka T, Abe S, Feng Q, Cui F, Watari F. Maturation of osteoblast-like SaoS2 induced by carbon nanotubes. Biomed Mater. 2009; 4:015005. [PubMed: 18981539]

Lum H, Roebuck KA. Oxidant stress and endothelial cell dysfunction. Am J Physiol Cell Physiol. 2001; 280:C719–741. [PubMed: 11245588]

Mehta D, Malik AB. Signaling mechanisms regulating endothelial permeability. Physiol Rev. 2006; 86:279–367. [PubMed: 16371600]

Misra SK, Ansari T, Mohn D, Valappil SP, Brunner TJ, Stark WJ, Roy I, Knowles JC, Sibbons PD, Jones EV, Boccaccini AR, Salih V. Effect of nanoparticulate bioactive glass particles on bioactivity and cytocompatibility of poly(3-hydroxybutyrate) composites. J R Soc Interface. 2010; 7:453–465. [PubMed: 19640877]

Monteiro-Riviere NA, Nemanich RJ, Inman AO, Wang YY, Riviere JE. Multi-walled carbon nanotube interactions with human epidermal keratinocytes. Toxicology Letters. 2005; 155:377–384. [PubMed: 15649621]

Nel A, Xia T, Madler L, Li N. Toxic potential of materials at the nanolevel. Science. 2006; 311:622–627. [PubMed: 16456071]

Pacurari M, Castranova V, Vallyathan V. Single- and multi-wall carbon nanotubes versus asbestos: are the carbon nanotubes a new health risk to humans? J Toxicol Environ Health A. 2010; 73:378–395. [PubMed: 20155580]

Pantarotto D, Briand JP, Prato M, Bianco A. Translocation of bioactive peptides across cell membranes by carbon nanotubes. Chemical Communications. 2004; (1):16–17. [PubMed: 14737310]

Patlolla A, Knighten B, Tchounwou P. Multi-walled carbon nanotubes induce cytotoxicity, genotoxicity and apoptosis in normal human dermal fibroblast cells. Ethn Dis. 2010; 20:S1-65–72. [PubMed: 20521388]

Podesta JE, Al-Jamal KT, Herrero MA, Tian B, Ali-Boucetta H, Hegde V, Bianco A, Prato M, Kostarelos K. Antitumor activity and prolonged survival by carbon-nanotube-mediated therapeutic siRNA silencing in a human lung xenograft model. Small. 2009; 5:1176–1185. [PubMed: 19306454]

Poland CA, Duffin R, Kinloch I, Maynard A, Wallace WA, Seaton A, Stone V, Brown S, Macnee W, Donaldson K. Carbon nanotubes introduced into the abdominal cavity of mice show asbestos-like pathogenicity in a pilot study. Nat Nanotechnol. 2008; 3:423–428. [PubMed: 18654567]

Porter D, Sriram K, Wolfarth M, Jefferson A, Schwegler-Berry D, Andrew M, Castranova V. A biocompatible medium for nanoparticle dispersion. Nanotoxicology. 2008; 2:144–154.

Porter DW, Hubbs AF, Mercer RR, Wu N, Wolfarth MG, Sriram K, Leonard S, Battelli L, Schwegler-Berry D, Friend S, Andrew M, Chen BT, Tsuruoka S, Endo M, Castranova V. Mouse pulmonary dose- and time course-responses induced by exposure to multi-walled carbon nanotubes. Toxicology. 2010; 269:136–147. [PubMed: 19857541]

Qian Y, Ducatman A, Ward R, Leonard S, Bukowski V, Lan Guo N, Shi X, Vallyathan V, Castranova V. Perfluorooctane sulfonate (PFOS) induces reactive oxygen species (ROS) production in human

microvascular endothelial cells: role in endothelial permeability. J Toxicol Environ Health A. 2010; 73:819–836. [PubMed: 20391123]

Qian Y, Liu KJ, Chen Y, Flynn DC, Castranova V, Shi X. Cdc42 regulates arsenic-induced NADPH oxidase activation and cell migration through actin filament reorganization. J Biol Chem. 2005; 280:3875–3884. [PubMed: 15492012]

Raffa V, Vittorio O, Ciofani G, Pensabene V, Cuschieri A. Cell Creeping and Controlled Migration by Magnetic Carbon Nanotubes. Nanoscale Res Lett. 2009; 5:257–262. [PubMed: 20651914]

Ruggiero A, Villa CH, Bander E, Rey DA, Bergkvist M, Batt CA, Manova-Todorova K, Deen WM, Scheinberg DA, McDevitt MR. Paradoxical glomerular filtration of carbon nanotubes. Proc Natl Acad Sci U S A. 2010a; 107:12369–12374. [PubMed: 20566862]

Ruggiero A, Villa CH, Holland JP, Sprinkle SR, May C, Lewis JS, Scheinberg DA, McDevitt MR. Imaging and treating tumor vasculature with targeted radiolabeled carbon nanotubes. Int J Nanomedicine. 2010b; 5:783–802. [PubMed: 21042424]

Shao R, Guo X. Human microvascular endothelial cells immortalized with human telomerase catalytic protein: a model for the study of in vitro angiogenesis. Biochem Biophys Res Commun. 2004; 321:788–794. [PubMed: 15358096]

Shasby DM, Shasby SS, Sullivan JM, Peach MJ. Role of endothelial cell cytoskeleton in control of endothelial permeability. Circulation Research. 1982; 51:657–661. [PubMed: 6890416]

Singh R, Pantarotto D, Lacerda L, Pastorin G, Klumpp C, Prato M, Bianco A, Kostarelos K. Tissue biodistribution and blood clearance rates of intravenously administered carbon nanotube radiotracers. Proceedings of the National Academy of Sciences of the United States of America. 2006; 103:3357–3362. [PubMed: 16492781]

Strieter RM, Mehrad B. New mechanisms of pulmonary fibrosis. Chest. 2009; 136:1364–1370. [PubMed: 19892675]

Takagi A, Hirose A, Nishimura T, Fukumori N, Ogata A, Ohashi N, Kitajima S, Kanno J. Induction of mesothelioma in p53+/- mouse by intraperitoneal application of multi-wall carbon nanotube. Journal of Toxicological Sciences. 2008; 33:105–116. [PubMed: 18303189]

Wallace WA, Fitch PM, Simpson AJ, Howie SE. Inflammation-associated remodelling and fibrosis in the lung - a process and an end point. Int J Exp Pathol. 2007; 88:103–110. [PubMed: 17408453]

Wang W, Watari F, Omori M, Liao S, Zhu Y, Yokoyama A, Uo M, Kimura H, Ohkubo A. Mechanical properties and biological behavior of carbon nanotube/polycarbosilane composites for implant materials. J Biomed Mater Res B Appl Biomater. 2007; 82:223–230. [PubMed: 17183562]

Wang X, Xia T, Ntim SA, Ji Z, George S, Meng H, Zhang H, Castranova V, Mitra S, Nel AE. Quantitative techniques for assessing and controlling the dispersion and biological effects of multiwalled carbon nanotubes in mammalian tissue culture cells. ACS Nano. 2010; 4(12):7241–52. [PubMed: 21067152]

Weber KS, Nelson PJ, Grone HJ, Weber C. Expression of CCR2 by endothelial cells : implications for MCP-1 mediated wound injury repair and In vivo inflammatory activation of endothelium. Arterioscler Thromb Vasc Biol. 1999; 19:2085–2093. [PubMed: 10479649]

Yadav SK, Bera T, Saxena PS, Maurya AK, Garbyal RS, Vajtai R, Ramachandrarao P, Srivastava A. MWCNTs as reinforcing agent to the hap-gel nanocomposite for artificial bone grafting. J Biomed Mater Res A. 2010; 93:886–896. [PubMed: 19705464]

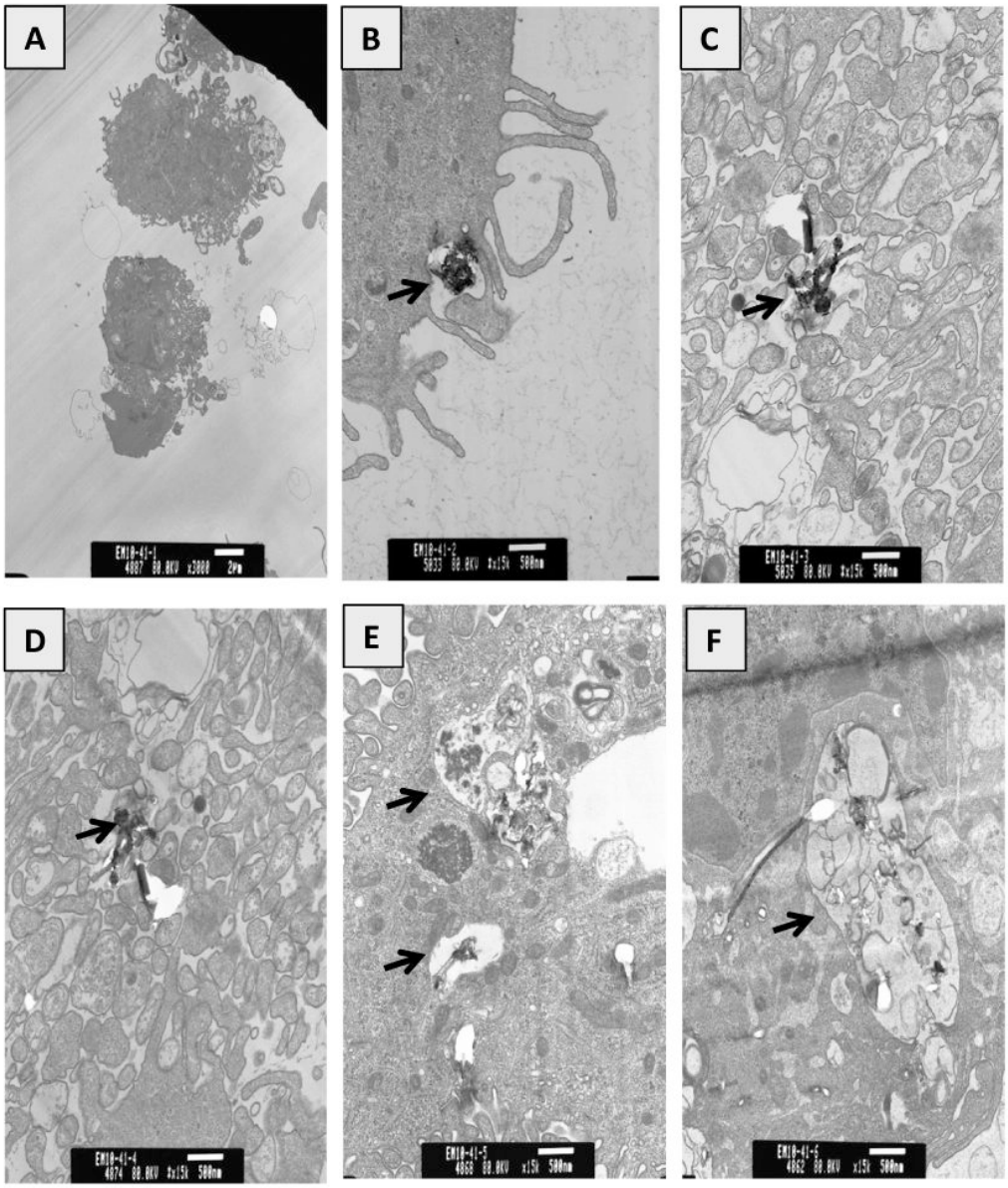

Figure 1.
Uptake of MWCNT by HMVEC. TEM micrographs of HMVEC exposed to MWCNT (2.5 μg/ml) for different periods of time ranging from 30 min to 24 hr. A) Control, B) 30 min, C) 1 hr, D) 4 hr, E) 8 hr, F) 24 hr. Arrows indicate MWCNT containing cytoplasmic vacuoles.

Figure 2A

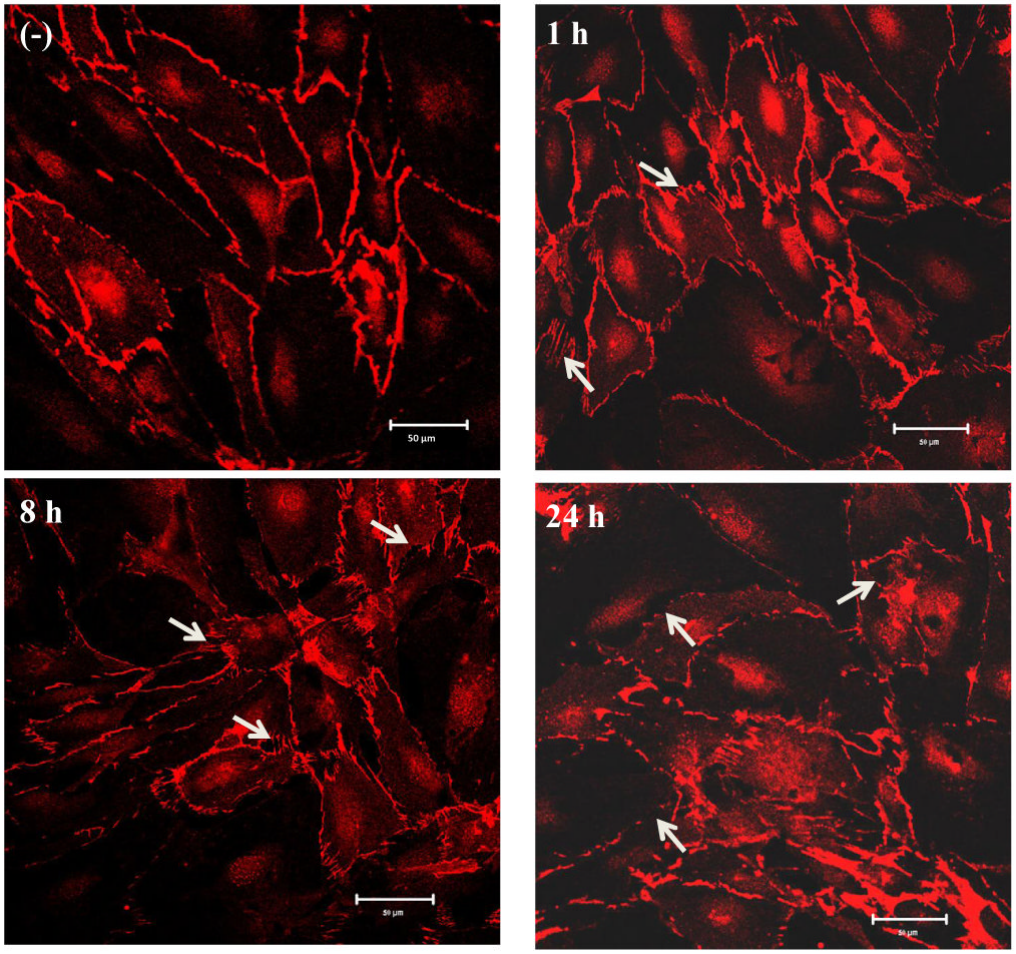

Figure 2B

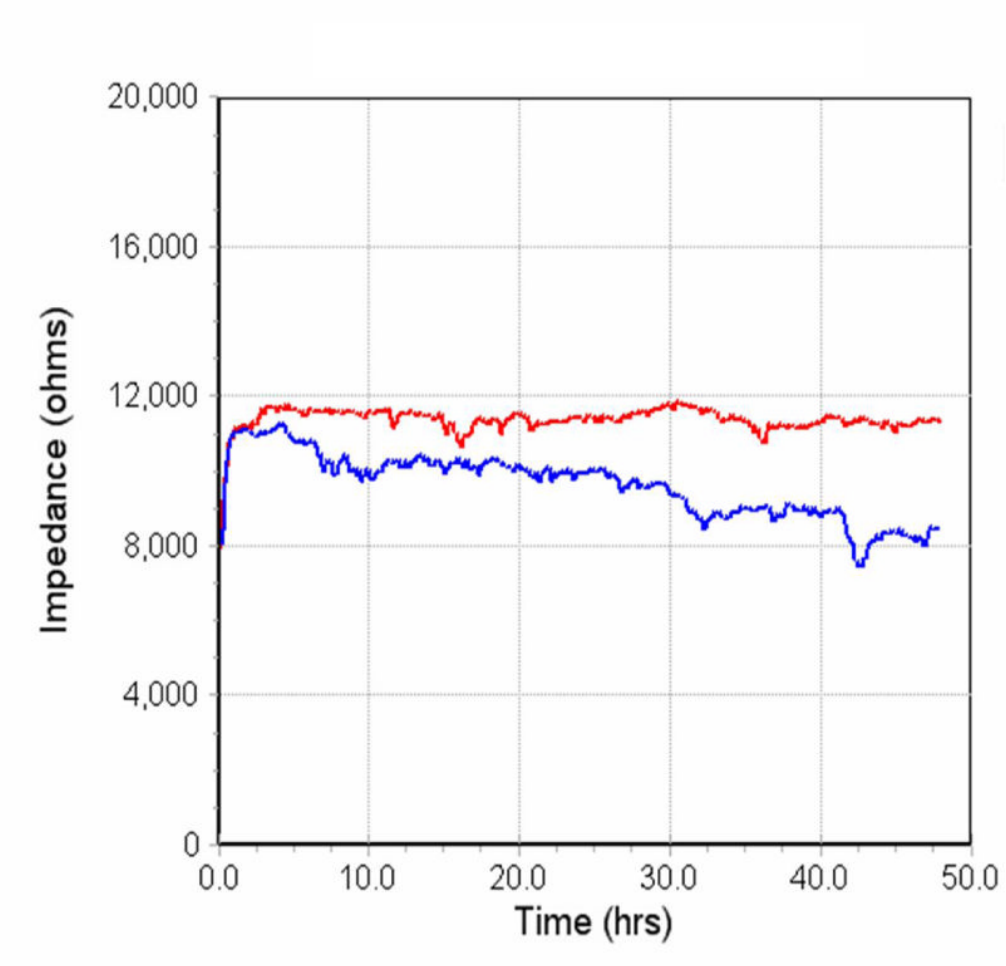

Figure 2.

MWCNT increase endothelial cell permeability. A) HMVEC were grown to confluent monolayers on cover slips, serum-starved, and treated with 2.5 μg/ml MWCNT for different periods of time as indicated. After treatment, cells were fixed, permeabilized, and stained with VE-cadherin antibody. A Zeiss confocal microscope was applied to take the images. Arrows indicate gaps in the HMVEC monolayer. Representative micrographs from three independent experiments are shown. (-) unexposed control cells. B) HMVEC were grown to a confluent monolayer on gold microelectrodes, serum-starved, and treated with 2.5 μg/ml MWCNT. TER was measured for 50 hr. Scale bar = 20 μm. Red line represents unexposed control cells and blue line represents MWCNT-exposed cells. Shown here is a representative graph from three independent experiments.

Figure 3A

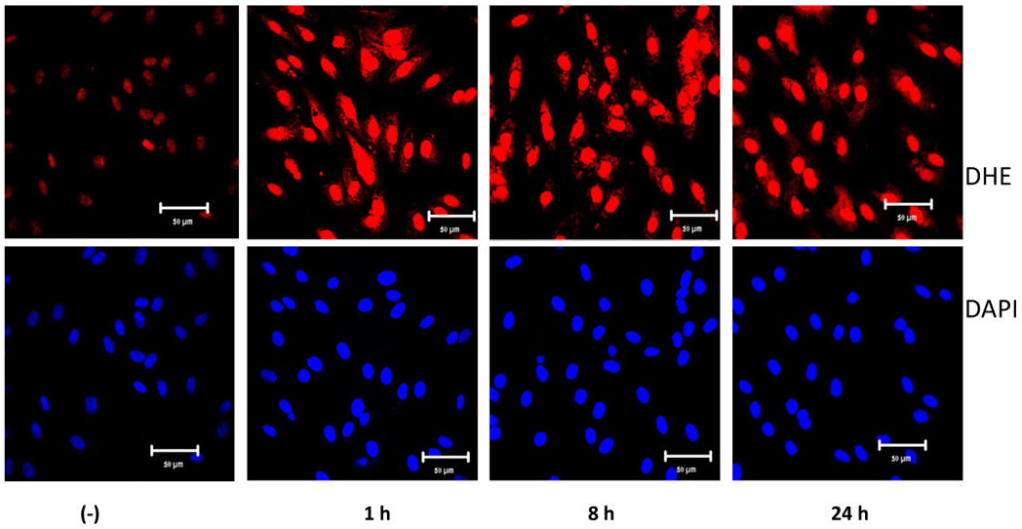

Figure 3B

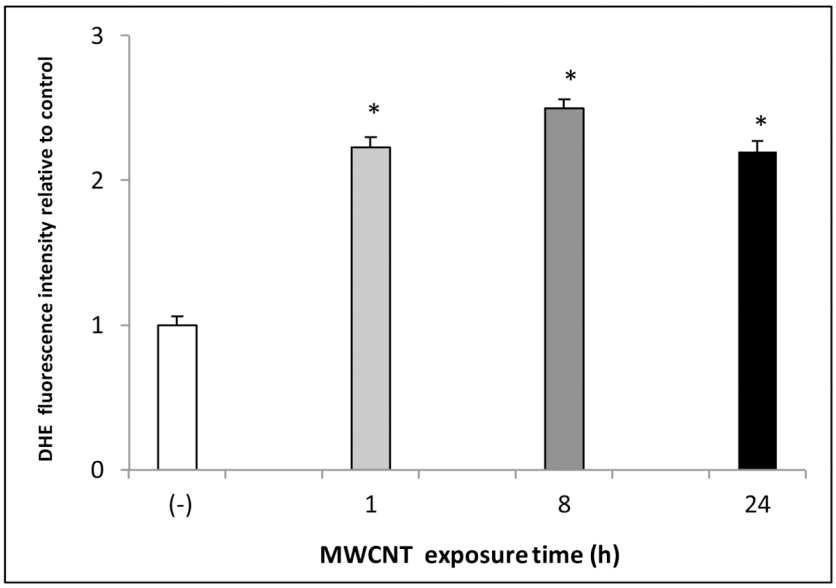

Figure 3C

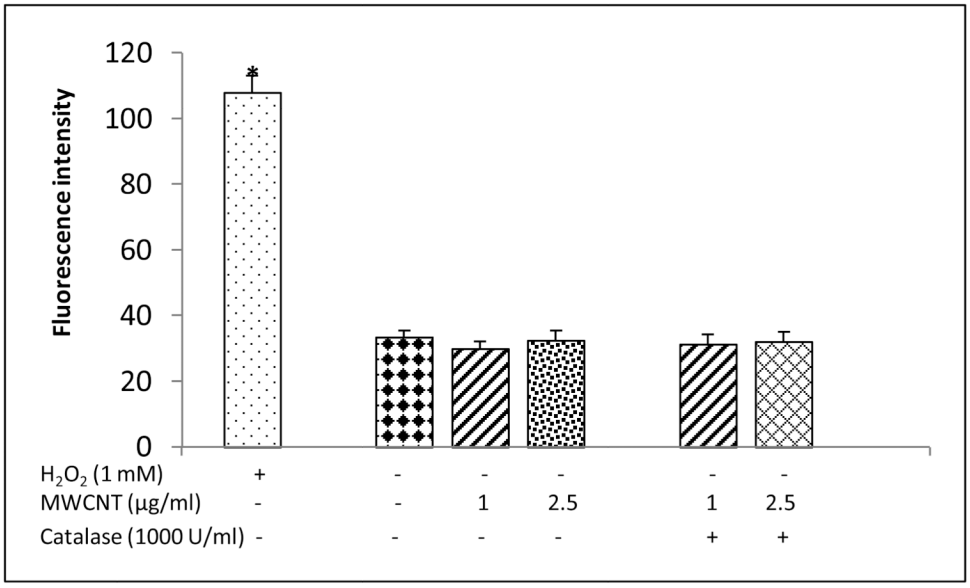

Figure 3D

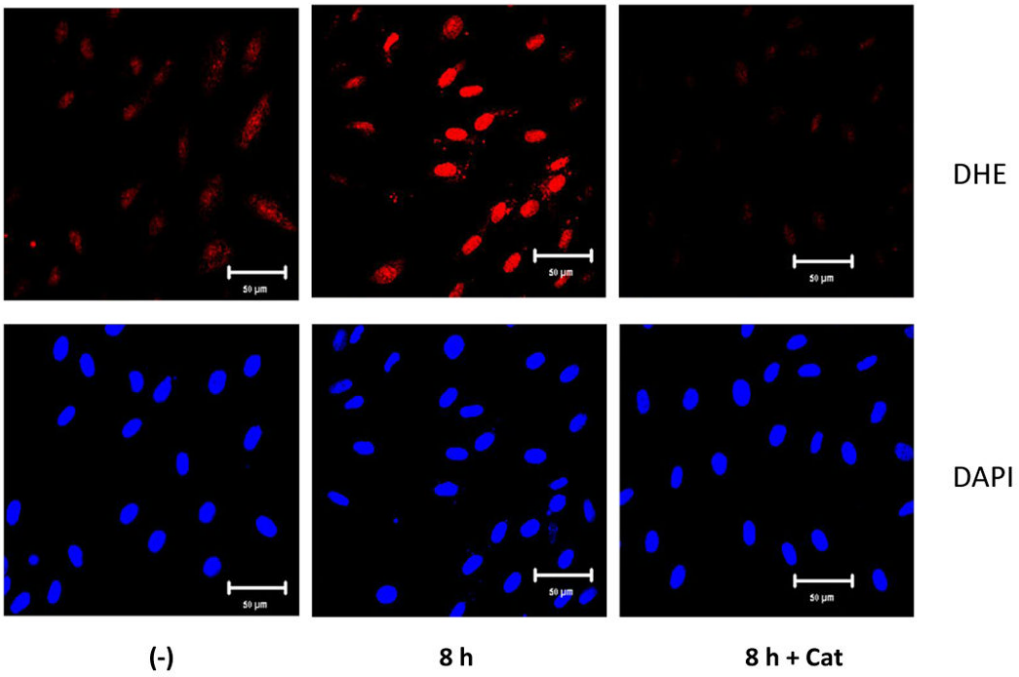

Figure 3E

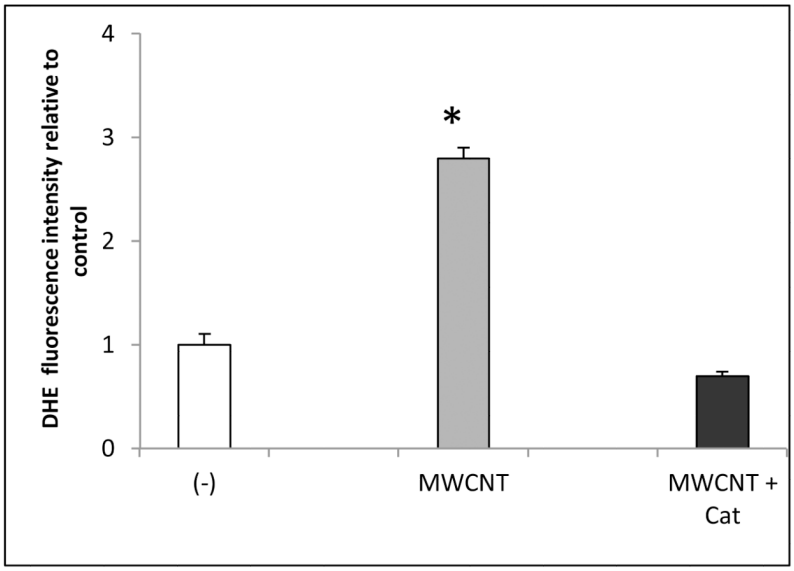

Figure 3.

MWCNT induce the production of ROS. A) HMVEC were grown on cover slips, serum-starved, and treated with MWCNT (2.5 μg/ml) for different periods of time as indicated. The production of ROS was determined by pre-treating the cells with DHE as described in Materials and Methods. DAP1 was used to stain cell nuclei. Shown here are representative micrographs from three independent experiments. Scale bar = 50 μm. B) Time-course of ROS production. DHE fluorescence intensity of MWCNT-treated samples relative to non-treated control samples was determined as described in Materials and Methods. Data (mean ± SEM) are representatives of three independent experiments. *, t-test, $p \leq 0.05$ versus control, n = 3. C) MWCNT do not induce ROS production in a cell-free system. DHE (5 μM) was mixed with H_2O_2, MWCNT, or catalase as indicated, followed by measurement of the fluorescence intensity of oxidized DHE using a cytoflour series 4000 fluorescence plate reader. Data represent means ± SEM of three experiments. *, significant at $p \leq 0.05$, t-test. D) HMVEC were grown on cover slips, serum-starved, and treated with 2.5 μg/ml MWCNT with or without catalase pretreatment (1000 U/ml) for 8 hr. The production of ROS was determined according to the methods described in Materials and Methods. DAP1 was used to stain cell nuclei. E) Catalase pretreatment (1000 U/ml for 8 hr) inhibits MWCNT (2.5 μg/ml)-induced ROS production in HMVEC. DHE fluorescence intensity was determined as described in Materials and Methods. Data (mean ± SEM) are representatives of three independent experiments. *, t-test, $p \leq 0.05$ versus non-treated control, n = 3. DHE = dihyroethidium, DAPI = 4′,6-diamidino-2-phenylindole.

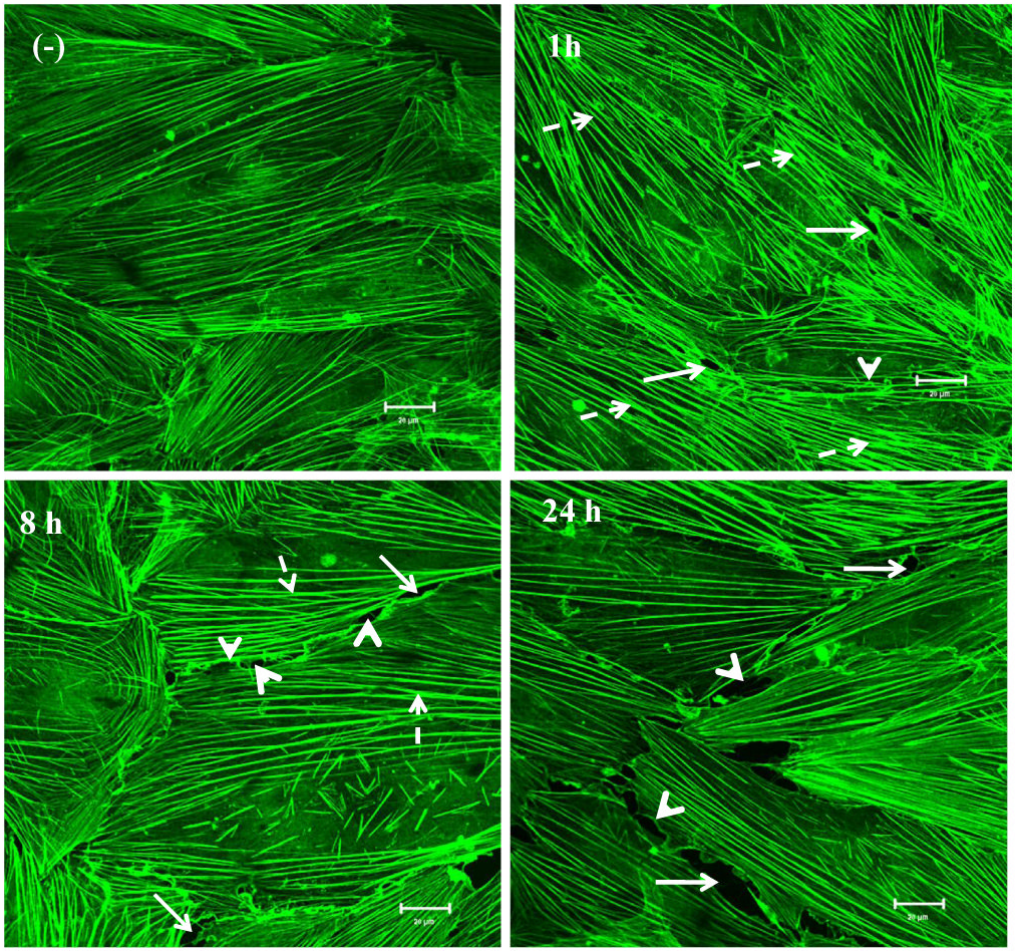

Figure 4.
MWCNT induce actin filament remodeling. HMVEC cells were grown on cover slips, serum-starved, and treated with 2.5 μg/ml MWCNT for different periods of time as indicated. After treatment, the cells were fixed, permeabilized, and stained with Alexa-546 phalloidin for actin filaments, followed by confocal microscopy analysis. Arrows indicate gaps; broken arrows indicate stress fibers (contractile bundles of actin filaments); arrow heads indicate lamellipodia (a meshwork of actin filaments at the cell periphery) and filopodia (actin-rich surface protrusions). Shown here are representative micrographs from three independent experiments. Scale bars = 20 μm.

Figure 5A

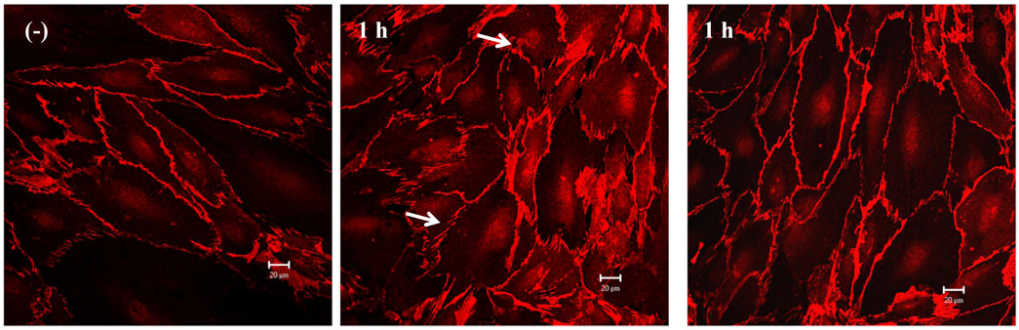

Figure 5B

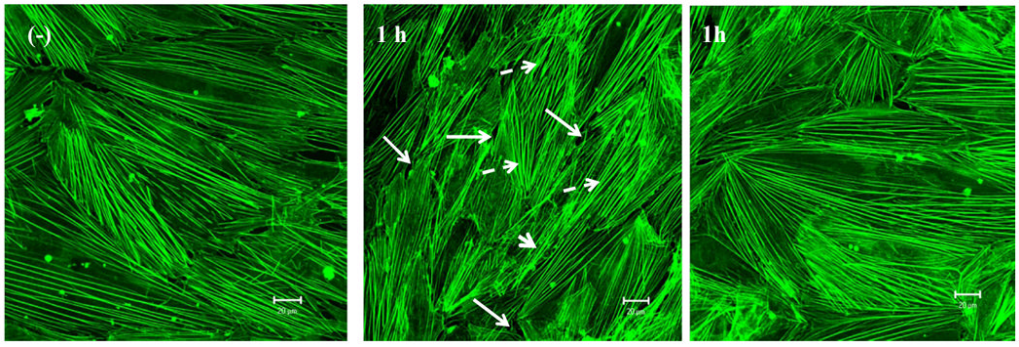

Figure 5.

ROS mediate MWCNT-induced endothelial cell permeability and actin filament remodeling. A) HMVEC were grown to a confluent monolayer on cover slips, serum-starved, and pretreated with catalase (1000 U/ml) for 30 min, followed by exposure to 2.5 μg/ml MWCNT for 1 hr. The change in permeability was determined according to the methods described in Figure 2. Arrows indicate gaps in HMVEC monolayer. B) HMVEC cells were grown on cover slips, serum-starved, and pretreated with catalase (1000 U/ml) for 30 min, followed by exposure to 2.5 μg/ml MWCNT for 1 hr. After the treatment, the cells were analyzed according to the methods described in Figure 4. Arrows indicate gaps; broken arrows indicate stress fibers; arrow heads indicate lamellipodia and filopodia. Shown here are representative micrographs from three independent experiments. Scale bars = 20 μm.

Figure 6

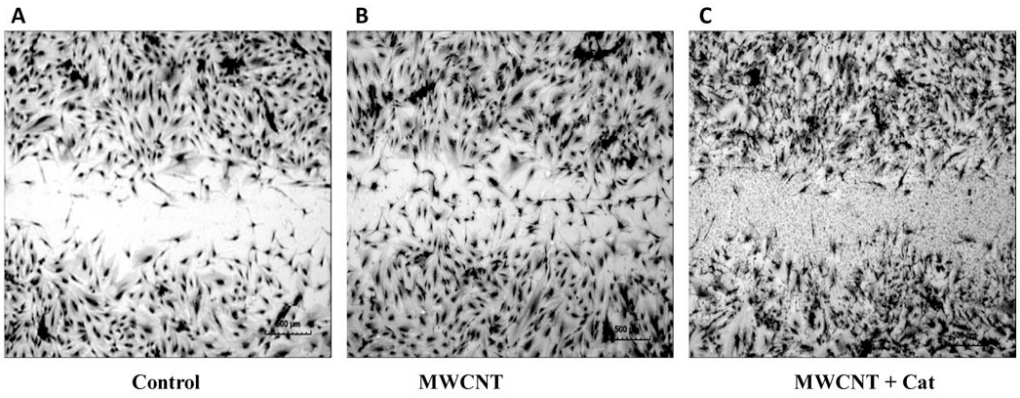

Figure 6D

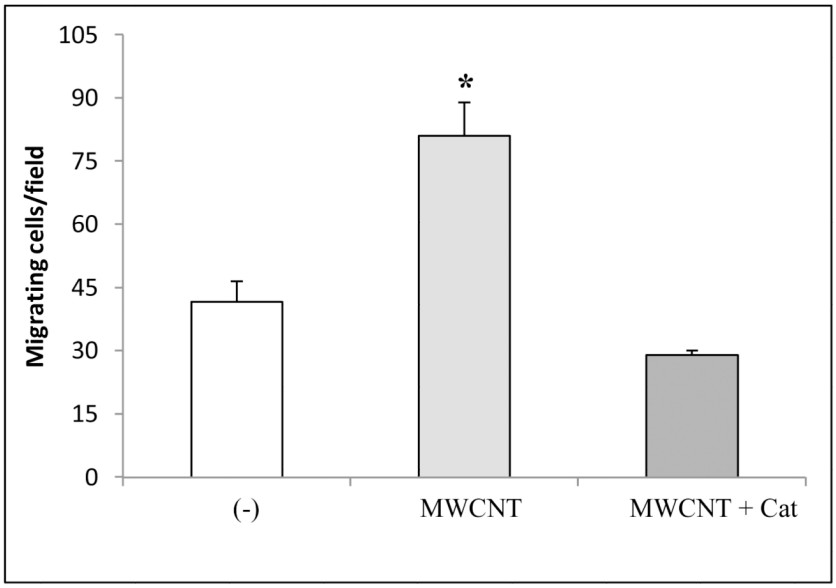

Figure 6.

MWCNT induce cell migration in HMVEC. A-C) HMVEC were grown to confluence, wounded, and exposed to: vehicle (A), 2.5 ug/ml MWCNT (B) or 2.5μg/ml MWCNT + 1000 U/ml catalase (C) for 24 hr. After these treatments, the cells were fixed, permeabilized, stained, and photomicrographed. Shown are representative micrographs from three independent experiments. Scale bar = 500 μm. D) The number of migrating endothelial cells was determined as described in Materials and Methods. Data (mean ± SEM) are representatives of three independent experiments. *, t-test, $p \leq 0.05$ versus non-treated control, n = 3.

Figure 7A

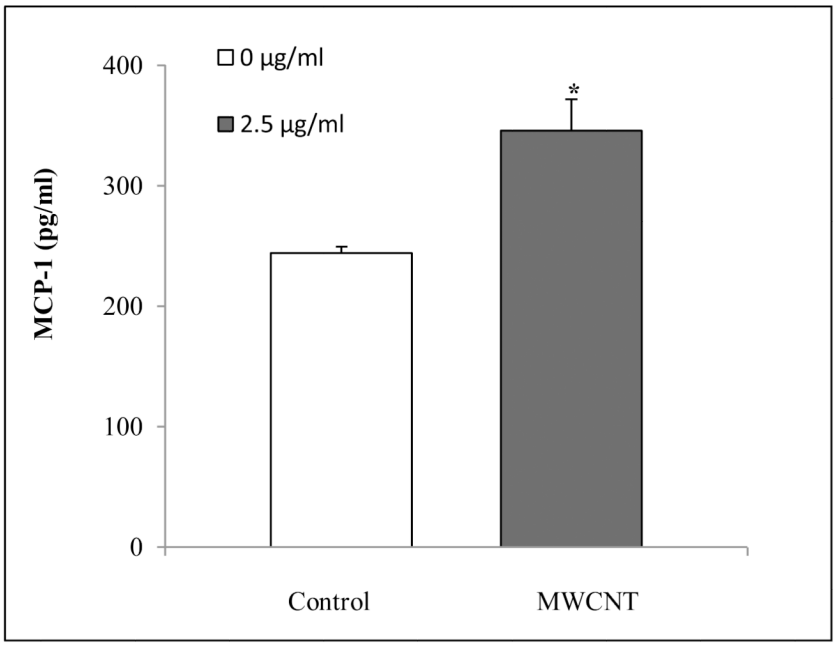

Figure 7B

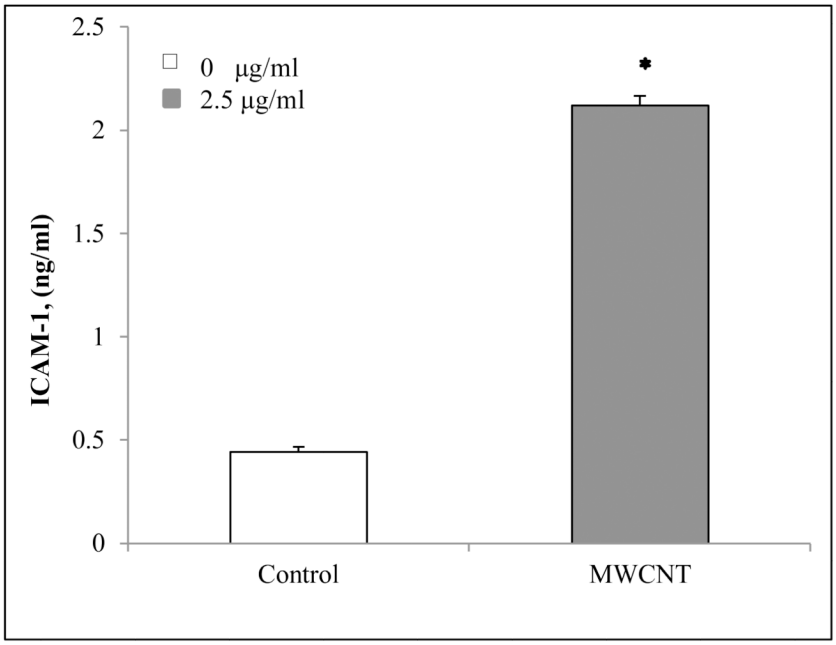

Figure 7.

MWCNT stimulate MCP-1 and ICAM-1 production in HMVEC. A) HMVEC were grown to a confluent monolayer and treated with vehicle or 2.5 µg/ml MWCNT for 24 hr. MCP-1 level was determined as described in Materials and Methods. Data (mean ± SEM) are representatives of three independent experiments. *, t-test, $p \leq 0.05$ versus non-treated control, n = 3. B) HMVEC were grown to a confluent monolayer and treated with vehicle or

2.5 μg/ml MWCNT for 8 hr. ICAM-1 level was determined as described in Materials and Methods. Data (mean ± SEM) are representatives of three independent experiments. *, t-test, $p \leq 0.05$ versus non-treated control, n = 3.